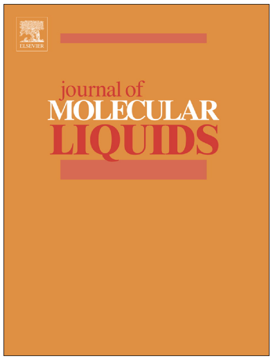

Bio-inspired N,S-doped siligraphenes as novel metal-free catalysts for removal of dyes in the dark

Leila Seifikar Gomi, Maryam Afsharpour, Mitra Ghasemzadeh, Panagiotis Lianos

PII: S0167-7322(19)33935-2

DOI: https://doi.org/10.1016/j.molliq.2019.111657

Reference: MOLLIQ 111657

To appear in: *Journal of Molecular Liquids*

Received date: 15 July 2019

Revised date: 13 August 2019

Accepted date: 28 August 2019

Please cite this article as: L.S. Gomi, M. Afsharpour, M. Ghasemzadeh, et al., Bio-inspired N,S-doped siligraphenes as novel metal-free catalysts for removal of dyes in the dark, *Journal of Molecular Liquids*(2019), https://doi.org/10.1016/j.molliq.2019.111657

Bio-inspired N,S-Doped Siligraphenes as Novel Metal-Free Catalysts for Removal of Dyes in the dark

Leila Seifikar Gomi[a], Maryam Afsharpour[a],*, Mitra Ghasemzadeh[a], Panagiotis Lianos[b]

[a] *Department of Inorganic Chemistry, Chemistry & Chemical Engineering Research Center of Iran, 14335-186, Tehran, Iran*

[b] *Department of Chemical Engineering, University of Patras, 26500 Patras, Greece*

***Corresponding author:** Tel: +98 21 44787720; Fax: +98 21 44787812

E-mail address: afsharpour@ccerci.ac.ir

Abstract

Bio-inspired porous Siligraphene (graphene-like SiC) catalyst and its N and N,S-doped SiC variants were synthesized via a low-temperature magnesiothermic method using natural precursors. The synthesized SiC catalysts were tested for the removal of anionic azo dyes (Congo red, Methyl orange, and Methyl red) in the dark. Si atoms in the siligraphene structure are more positive than C atoms due to the electronegativity of the latter. In doped structure, insertion of N and S atoms can further increase the positive charge of Si atoms and improve adsorption of oxygen and of the above anionic dyes on the surface of SiC. Thus, the catalytic activity of doped SiC for degradation of the dyes increased. A mechanism is proposed where O_2 molecules chemisorb onto the surface of SiC, O-O bond length elongates, oxygen bond dissociates and radicals are produced. Quenching experiments show that $^{\bullet}O_2^-$ and $^{\bullet}OH$ radicals are the main reactive species in this process. Doping of nitrogen and sulphur in the presence of Si atoms in siligraphene structure has been shown to improve its capacity for dye removal compared to the corresponding carbon catalysts. Moreover, the SiC catalysts display good stability so that their performance did not significantly decrease even in continuous operation.

Keywords: Siligraphene; N and S doping; Metal-free catalyst; Dye Removal.

1. Introduction

As a result of rapid growth of world population, water purification processes make the most important challenges for researchers in wastewater management [1-4]. Organic dyes are a main source of water pollution and they have a negative impact on human health both directly and indirectly [5,6]. It is therefore essential to remove these pollutants from wastewater. Current research has developed several advanced processes for dye removal. Among them, removal by adsorption of dyes constitutes a powerful tool of great practical importance. Numerous porous materials have been employed for this purpose such as zeolites, biopolymers, silica, alumina, carbon and even Sahara desert sand [7-12].

As far as we know, there is only one reference on the use of silicon carbide (SiC) to remove methylene blue dye by adsorption [13], although there are some literatures on adsorption or photocatalytic degradation of dyes using SiC composites with metal or metal oxides [14-16]. Silicon carbide is one of the most useful compounds due to its specific properties such as thermal and chemical conductivity, great mechanical strength, good chemical inertness, and oxidation resistance [17-19]. Therefore, SiC is broadly used in sensors, drug delivery systems, composites, heterogeneous catalysts, hydrogen storage, electronic, and optical devices [20-23]. In addition, previous reports show that SiC with siligraphene structure has interesting properties due to its surface charge density [24,25]. SiC has been synthesized by several methods including sol-gel, pyrolysis of carbon-containing siloxane polymers, and electrochemical etching of SiC wafers [26,27]. All these methods are unable to control the morphology of silicon carbide nanostructures due to their high process temperature (>1200℃). Also, these synthesis processes are costly energy consumers using not environmentally friendly material precursors. In this respect, magnesiothermic method has been recently suggested as a low-temperature method (600-800°C) for preparing SiC nanostructures which allowed to control the morphology and production of porous materials. In this method, silica in the presence of Mg turns to silicon and because of this highly exothermic reaction, silicon carbide can be synthesized at lower temperature [28,29]. In addition in the present work, we have chosen cost effective porous natural precursors to produce green porous SiC [24,30].

In this study, we report the synthesis of bio-inspired porous SiC and its doped structures via magnesiothermic method. Diatomaceous earth and glucose were used as natural silicon and carbon source, respectively. Surface area and chemical heterogeneities of absorbents are important for efficient adsorption and also catalytic performance [31]. Thus, the effect of dopants on the adsorption capacity and the catalytic performance of porous SiC has been investigated. In addition, a new mechanism of advanced oxidation process is reported for dye degradation. In summary, the advantages of the presently proposed SiC catalysts are the use of natural precursors for their synthesis, the relatively low temperature synthesis procedure, and the mild conditions for their operation, i.e. dark, ambient temperature and lack of additional oxidants.

2. Experimental

2.1. Materials

Diatomaceous earth (SiO_2 content: 98%, porosity >93%, Density: 120g/L, pH: 7.8) was used as Si source. Glucose, urea, and thiourea were purchased from Merck and used as C, N, and N-S sources. Magnesium powder in the size of 0.06–0.3 mm (Merck) was used in the synthesis of SiC (magnesiothermic method). Hydrofluoric acid and hydrochloric acid were used to wash magnesium and unreacted silica. Congo red (C.I. Direct Red 28), Methyl Red (C.I. Acid Red 2), and Methyl orange (C.I. Acid Orange 52 were used as the anionic azo dyes.

2.2. Synthesis of SiC, N-doped SiC, and N, S-doped SiC samples

Diatomaceous earth was first washed with 1 M HCl solution to remove impurities, and dried in an oven at 60 °C for 12 h. Then, 2 g of washed diatomaceous earth was dispersed in a 250 ml of 8 g/L glucose solution (C source) and sonicated 5 times for 15 min for better penetration of glucose in the pores of diatomaceous earth. The mixture was put in an oven and dried at 70 °C for 24 h. For the synthesis of SiC samples, the dried mixture was carbonized at 700 °C for 1 h under an N_2 atmosphere (5º C/min). Afterward, SiO_2/C composite was sufficiently mixed with magnesium powder in Si:Mg molar ratio of 1:2 and put it in a furnace at 700 ºC for 5 h under N_2 atmosphere to produce SiC sample. Finally, to remove the magnesium oxide and its derivatives, the obtained SiC samples were immersed in a 2 M HCl solution for 24 h at room temperature. After washing it with water to remove magnesium chloride, the SiC product was immersed in a 2 M HF solution to remove unreacted silica. Then, the pure SiC sample was dried at 60°C for 24 h in a vacuum oven.

To synthesize the doped SiC samples, 0.8 g of urea or thiourea was added to the glucose solution and used to produce the N-doped and N,S-doped SiC according to the reported procedure, respectively. In this article, SiC, N-doped SiC, and N, S-doped SiC samples were briefly named SIC, N-SIC, AND NS-SIC, respectively.

2.3. Synthesis of carbon catalysts

Carbon catalysts were synthesized by heating glucose at 700 °C for 1 h under an N_2 atmosphere (5º C/min). Doped carbon catalysts were synthesized by adding 10 wt% of urea or thiourea to glucose as N or N-S sources.

2.4. Characterization and Methods

The morphologies of porous SiC samples were obtained on a TESCAN, VEGA3 scanning electron microscope (SEM) equipped with an X-ray energy dispersive spectroscope (EDX). Powder diffraction data were assembled by BrukerAxs, D8 Advance. The infrared spectroscopy was done by a Bruker, Vector instrument. N_2 adsorption/desorption isotherms and the pore size distributions were obtained from the Belsorp mini system. XPS analysis was performed on a Thermo Scientific, ESCALAB 250Xi system using a spectrometer with MgK_α radiation (1253.6 eV). Raman spectroscopy was done by a Bruker, Senterra micro-Raman (785 nm laser wavelength). Dye removal tests were performed with a Perkin-Elmer, Lambda-35 UV-Vis spectrometer.

All the calculations were done by the Gaussian 03 program. First, the structures were optimized at the BP86/6-31+G** level and then NBO calculations were carried out using NBO 3.1 in order to obtain the atomic charges.

2.5. Methods for Dye Removal

Batch experiments were carried out in the dark at ambient temperature in the presence of SiC catalysts (SiC, N-SiC, and NS-SiC samples). Different concentrations of Congo red dye (30, 50, 70, and 100 ppm) were prepared to test the removal capacity of SiC samples. 0.01 g of synthesized SiC samples were dispersed in 10 ml of certain dye solution under stirring (120 rpm) in a dark chamber. Air as a supply of oxygen was bubbled to the system to saturate the solution with oxygen during the reaction. The concentration of dye in solution was measured by UV-Vis spectroscopy at 500 nm after each 5 min.

All of the experiments were repeated three times to ensure data accuracy. The amount of dye removal (Q_e) was determined using the following equations:

$$Q_e = (C_0 - C_e)\, V/M \qquad (1)$$

$$\text{Removal \%} = (C_0 - C_e)/C_0 * 100 \qquad (2)$$

Where C_0 and Ce are the initial and equilibrium dye concentrations (mg L^{-1}), M is the mass of SiC samples (g), and V is the volume of dye solutions (L).

In addition to Congo red, Methyl red and Methyl orange anionic azo dyes were also tested to evaluate the activity of the SiC catalyst.

Quenching experiments were done by introducing 2 mM of IPA (isopropanol), BQ (p-benzoquinone), and AO (ammonium oxalate) as $^{\bullet}OH$, $^{\bullet}O_2^{-}$, and h^+ quenchers respectively.

3. Result and Discussion

3.1. Characterization

FT-IR spectra for SiC, N-SiC, and NS-SiC samples are shown in Fig. 1. Peaks appearing at 816, 822, and 819 cm^{-1} are related to the Si-C stretching vibration in SiC, N-

SiC, and NS-SiC silicon carbide samples, respectively. The peaks that were observed at 3420 cm^{-1} in all samples can be mainly assigned to the O-H stretching vibration of oxygen-functional groups and chemisorbed water on the surface of SiC.

XPS analysis of synthesized SiC samples is recorded in Fig. 2a-h. XPS survey spectra of all samples showed Si2p (includes Si2p 3/2 and Si2p 1/2), C1s, and O1s peaks which indicate the presence of SiC associated with oxygen-containing functional groups. The Si2p 3/2 XPS spectra for SiC sample (Fig. 2a) can be deconvoluted into two bands at 99.31 and 100.82 eV, corresponding to Si-Si and Si-C species, respectively. This result shows the presence of silicon in the SiC sample. While, the Si2p XPS peaks of N-SiC and NS-SiC sample were fitted to two bonds that are related to Si-C and O-Si-C species at about 101 and 102 eV, respectively (Fig. 2c,e). The C1s peaks of N-SiC and NS-SiC show C-Si, C-C, and C-N bonds at about 283, 284.5, and 286 eV, respectively (Fig. 2d,f). The N1s XPS peaks in N-SiC and NS-SiC (Fig. 2g,h) show doublet peaks at about 398 and 400 eV for pyridinic and pyrrolic nitrogen, respectively. The S2p XPS peak of NS-SiC is attributed to the C-S-C bond (169.54 eV) (Fig. 2i).

The surface atomic percentage of Si, C, O, N, and S for SiC, N-SiC, and NS-SiC samples that were obtained from EDX analysis and derived from the corresponding peak areas of XPS spectra are summarized in Table 1. The results show that the presently prepared SiC samples mainly consist of Si, C, and O elements. The co-doped NS-SiC sample shows a higher N concentration (5.66 atom%) than the singly N-doped sample (N-SiC) (4.05 atom%). The amount of sulfur in NS-SiC was measured to be about 0.54 atom%.

XRD patterns of SiC samples are depicted in Fig. 3. XRD patterns of SiC, N-SiC, and NS-SiC show peaks at about 2θ = 33.86, 35.57, 37.95, 41.32, 60.04, and 71.78° that are assigned to (101), (102), (103), (104), (110), and (202) planes of 6H-SiC structure (JCPDS 29-1128). Also, in SiC sample, three diffraction peaks were observed at 2θ = 28.39, 47.26, and 56.07° can be contributed to the (111), (220), and (311) planes of cubic phase of silicon (JCPDS 27-1402).

Raman spectra of synthesized SiC catalysts are shown in Fig. 4. In all samples, two specified bands of graphene, D bond at about 1350 cm^{-1} and G band at about 1570 cm^{-1} were observed. The presence of these two peaks on the structure of SiC samples demonstrate the formation of siligraphene structure [24]. The siligraphene is a graphene-like structure with high amount of Si elements that are doped in carbon with graphene structure [32-34].

As we know, the D band is activated by lattice defects such as substitution of heteroatoms, vacancies, or functional groups on the surface of graphene structures. So, the intensity ratio of peaks D to G can indicate the degree of disorder and amount of sp^2 in a sp^3 network. The I_D/I_G ratio in SiC, N-SiC, and NS-SiC were found to be 0.92, 0.93, and 0.95, respectively. The larger I_D/I_G ratio can result from more defects in doped structures due to the substitution of doped atoms in the carbon skeletons. So, NS-SiC attained the highest I_D/I_G value due to the largest amount of dopants.

SEM images of synthesized SiC samples (SiC, N-SiC, and NS-SiC) are shown in Fig. 5b-d. Fig. 5a presents the morphology of silicon precursor (diatomaceous earth). The SEM of SiC sample (SiC without doping) clearly shows a porous structure like to its initial precursor (diatomaceous earth) (Fig. 5b). It was concluded that the diatomaceous earth performed as hard template for the synthesis of the porous SiC sample. By adding nitrogen and sulfur in the SiC matrix, the morphologies of N-SiC and NS-SiC were changed and a different porosity was observed (Fig. 5c,d).

The porosity of prepared SiC samples was studied by N_2 adsorption/desorption measurements which demonstrated a type IV isotherm that illustrates the presence of micro and mesopores (Fig. 6). The specific surface areas of SiC, N-SiC, and NS-SiC were found to be 101, 135, and 133 m^2/g, respectively. The results show that the surface area increased after doping the elements in the SiC structure. It can be attributed to the interaction between the N and S sources and glucose which forms a new matrix with higher porosity. As shown in Table 2, NS-SiC show a significant increase in the micropore content (14.73%). NS-SiC sample shows the lowest total pore volume (0.291 cm^3/g) and pore diameter (8.759 nm) due to the higher nitrogen and sulfur dopant contents.

3.2. Dye Removal Results

Fig. 7 shows the removal of Congo red using SiC catalysts with different initial concentrations of dye (30-100 ppm). All the experiments were done at an optimized amount of catalyst in the dark under air bubbling to saturate the solution with oxygen (Table 3). The amount of dye adsorbed (*Qe*), equilibrium concentrations (*Ce*), time of removal, and the percentage of dye removal are given in Table 3. Both doped-SiC catalysts can completely remove lower concentration of dye after a short time (5 min). Based on catalytic data, it was revealed that the removal percentage was decreased by increasing the initial concentration of dye. Also, it is obvious that by increasing the concentration of the dye, the differences in catalytic performances of synthesized SiCs were better observed. Results clearly show that doping the heteroatoms increases the catalytic property in the removal of dye in the order NS-SiC > N-SiC > SiC.

Fig. S1 and Table S1 illustrated the rate of adsorption/degradation of the Congo red dye on the NS-SiC catalyst which was fitted by three kinetic models, including pseudo-zero-order, pseudo-first-order, and pseudo-second-order models to obtain better understanding of this process. As can be seen in Fig. S1, the highest correlation coefficient (R^2) of Congo red adsorption/degradation was related to the pseudo-second-order kinetic. Therefore, the removal process of Congo red by SiC catalyst was followed by the pseudo-second-order kinetic model.

As dye removal reactions were performed in the dark, no photocatalytic reactions could occur. Congo red is adsorbed on positive sites of SiC samples through the oxygen atoms of the sulfonate group of dye molecules. More adsorptions can occur in N-SiC and NS-SiC samples due to their higher surface areas than in the SiC sample. Also, doping the heteroatoms on the SiC matrix increases the defects and can enhance the adsorption.

However, the surface area of SiC catalysts was not very high (lower than 150 m^2/g), while results show that the dye can be completely removed in a short time. This indicates the existence of another mechanism besides adsorption. We then suggest a mechanism of dye degradation via oxidation processes by chemisorption of oxygen on the surface of SiC catalysts.

Fig. 7 also shows that NS-SiC can completely remove dye up to an initial concentration of 70 ppm. By increasing the concentration above 70 ppm, a decrease in removal percentage was observed. Obviously, a high dye concentration can lead to a saturation of the surface of the NS-SiC catalyst and limit oxygen adsorption thus decreasing catalytic activity.

3.3. Proposed Mechanism

In our proposed mechanism, the O_2 molecule chemisorbs to the surface of SiC samples by bonding with two adjacent silicon atoms and forms an epoxide like structure (Fig. 8). The Si-O bond length is a strong chemical bond and oxygen molecule can easily adsorb on the SiC surface. After chemisorption of O_2, the O-O bond length elongates and a charge transfer from SiC to O_2 occurs. Then the oxygen bond dissociates and $^{\bullet}O$, $^{\bullet}O_2^{-}$, $^{\bullet}OH$, or $^{\bullet}OOH$ radicals are produced. In another adsorption configuration, H_2O molecules can also adsorb on the SiC surface. As shown in Fig. 8, both O_2 and H_2O prefer to adsorb on the Si atoms that have a more positive charge. The H_2O molecule has a lower affinity for SiC surface and it may be physisorbed on the Si sites. When the water molecule is adsorbed, a proton in the H_2O molecule can be dissociated and forms OH groups by connecting to the dissociated O_2 molecules.

Theoretical study (Fig. 9) shows that the charge of Si atoms increases by doping the heteroatoms and the co-doped SiC then becomes more positive than. The charge of Si atoms was calculated to be about 1.96, 1.94, and 1.83 for NS-SiC, N-SiC, and SiC, respectively. Since the charge of Si atoms in the co-doped SiC is more positive, the NS-SiC shows the higher affinity for oxygen adsorption.

To prove the proposed mechanism, the catalytic test was repeated by purging N_2 and O_2 to evaluate the effect of oxygen in the removal of dye. The results show that purging oxygen into the system increases the rate of reaction and NS-SiC removed the Congo red (70 ppm) completely after 10 min (dye was removed in the air after 20 min). Purging N_2 shows a 42% dye removal, which is obviously related solely with dye adsorption.

In addition, quenching experiments were done to measure the effects of active species during the catalytic reaction. Fig. 10 clearly shows that in the presence of BQ as $^{\bullet}O_2^{-}$ quencher, the degradation of the dye was significantly limited, which suggest that the $^{\bullet}O_2^{-}$ radical is the main active species in the catalytic degradation of the dye. The result also reveals that the degradation of the dye was reduced by addition of IPA, which indicates the involvement of $^{\bullet}OH$ radical as a reactive species. However, h^{+} quenching by AO showed negligible effect on the removal of the dye (Fig. 10), thus suggesting the absence of any photocatalytic effect.

It is well known that the surface property of the catalyst is an important parameter in adsorption and catalytic activity. The doped SiC samples have more surface areas and show higher dye removal. Also, NS-SiC shows the highest removal due to the more N and S doping that should be attributed to the more positive charge on the Si atoms in SiC sample. Also, doping with heteroatoms can increase the affinity of SiC surface to oxygen groups and improve the catalytic properties.

As the charge surface is an important role in catalytic performance of doped-SiC, the effect of pH on dye removal was tested for NS-SiC catalyst (Fig. 11). The pH value of zero point charge (pHzpc) of NS-SiC catalyst is measured 6.91. It is well-known that in the pH higher than pHzpc of catalyst, the surface of catalyst became positive which is proper for adsorption of negative dyes and oxygen species. So, the best dye removal results was observed at pH higher than 7. The decrease of removal in lower pH can be attributed to decomposition of dye.

Fig. 12 shows the UV-Vis spectra that were plotted during the removal process of 100 ppm dye solution. Results show the intensities of all peaks in Congo red dye were which confirms the destruction of azo-linkage (500 nm) and also, the benzoic (235 nm), and naphthalene rings (347 nm) in Congo red structure. Furthermore, no new bands appeared in the UV-Vis region. Also, degradation products formed at the end of catalytic process were analyzed by LC–MS. Main species detected in the solution are presented in Fig. S1 including LC–MS spectra for the aqueous solution of 30 ppm Congo red dye which was reacted with NS-SiC for 10 min. Only two peaks at 135 and 143 m/z ratios was observed with a very low intensity which prove the significant decolorization and mineralization to give CO_2 and H_2O during this catalytic process.

3.4. Recovery of Catalysts

The reusability of the catalysts was tested by using treated and also washed catalysts. First, the catalysts were filtered from dye solution and used in another run without any further recovery (Fig. 13a). After 3 runs, only a little decrease was observed in the activities of SiC catalysts. It confirms that the catalysts, especially NS-SiC, can remove dye by degradation in addition to adsorption. These claims can be confirmed by FT-IR data (Fig. 13b). No obvious peaks were observed on the FT-IR spectra of used SiC catalysts after the first run, especially in the case of NS-SiC. This result shows that catalysts can completely degrade the dye, therefore, no dye residues were detected on the surface of the catalysts. However, after five runs, catalytic activities decrease due to the saturation of the surface of catalysts with adsorbed dye and this result to a decrease of dye degradation.

The recovery of NS-SiC catalyst was tested after washing with water (Fig. 14a). It shows no significant decrease in the activity of this catalyst after 5 runs. FTIR and diffuse reflectance spectra of washed NS-SiC catalyst were compared with fresh and used NS-SiC catalysts (Fig. 14b,c). Results confirm that no traces of dye remained on the surface of the catalyst and the chemical structure of the catalyst has not changed after the degradation experiment and washing process.

3.5. Comparison of Catalytic Activities

To better appreciate their catalytic activity, corresponding carbon catalysts were also synthesized. Fig. 15 shows the comparison of Congo red removal by using carbon and SiC catalysts. It is seen that all SiC catalysts show better catalytic properties than their corresponding carbon catalysts, although, dye removal was increased by doping the heteroatoms onto the carbon matrix. This effect of heteroatoms doping is also observed in the results of SiC catalysts.

Based on the proposed mechanism, the activities of SiC catalysts were compared with corresponding carbon catalysts (Fig. 15). Results clearly show the influence of doping of heteroatoms in catalytic properties. Carbon catalyst without doping can remove dye only by adsorption process. But, doped carbon catalysts can remove dye according to adsorption and oxidation reaction simultaneously. Doping N and S atoms in the graphene structure induces a positive charge on the carbon atoms which chemisorb oxygen molecules and produce radicals which assist oxidation process. Comparison of carbon with SiC catalysts showed higher catalytic performance in SiC catalysts due to the presence of Si atoms on the graphene structure. According to the proposed mechanism, the Si atoms in siligraphene structure are the active sites to adsorb oxygen molecules due to the higher positive charge. By doping heteroatoms into the siligraphene structure, their properties their properties are further enhanced due to the increase of the Si electropositivity. The positive charge on the Si atoms can chemisorb O_2 molecules from the solution and generate oxygen radicals which enhance the oxidation process and destroy the organic dye.

Two other anionic azo dyes (Methyl red and Methyl orange) were also tested for further evaluation of catalytic properties of doped SiC. For this reason, NS-SiC as the best catalyst was selected and the catalytic removal of Congo red was compared with Methyl red and Methyl orange (Fig. 16). As shown in Fig. 16, NS-SiC removed Congo red and Methyl orange completely after 10 min and removed 98% of methyl red after 15 min. These results confirm that this catalyst can remove different organic dyes via an oxidation process.

4. Conclusion

To illustrate the catalytic properties of silicon carbide nanostructures in the removal of anionic azo dyes, SiC, N- doped SiC, and N,S-doped SiC have been prepared from natural sources (diatomeous earth as Si and glucose as C sources). This study has been focused on the effect of doping onto the SiC with siligraphene structure. The obtained catalysts showed different textural properties, surface area, and catalytic properties. The catalytic results can be attributed to the fact that doping the N and S onto the SiC structure leads to an increase in surface area and the increase of defects which enhance the adsorption of dye. Furthermore, doping can increase the positive charge of Si atoms which can adsorb oxygen and then, degradation of dye may take place due oxidation processes. Also, the results of these SiC catalysts were compared with their corresponding carbon analogues. Results show that the N and S doping in the presence of Si atoms in the siligraphene structures enhance dye removal activities compared to the corresponding carbon catalysts. Moreover, the recyclability of the catalysts was evaluated after multiple uses. The SiC catalysts display good stability and especially in the N, S-doped SiC, the performance of the catalyst did not decrease significantly even in continues reaction. So, silicon carbides can be introduced as the high-performance metal-free catalysts in degradation of organic compounds.

Acknowledgment

Support of this investigation by Chemistry and Chemical Engineering Research Center of Iran is gratefully acknowledged.

Figure Caption:

Figure 1. FT-IR spectra of SiC, N-SiC, and NS-SiC samples.

Figure 2.XPS analysis of Si2p(a) and C1s(b) of SiC; Si2p(c), C1s(d), and N1s(g) of N-SiC; and Si2p(e), C1s(f), N1s(h), and S2p(i)of NS-SiC samples.

Figure 3. XRD patterns of SiC, N-SiC, and NS-SiC samples.

Figure 4. Raman spectra of SiC, N-SiC, and NS-SiC samples.

Figure 5. SEM images of Diatomaceous earth (a), SiC (b), N-SiC (c), and NS-SiC (d) samples.

Figure 6. N_2 adsorption/desorption isotherms of SiC (a), N-SiC (b), and NS-SiC (c), and pore size distribution of SiC (d), N-SiC (e), and NS-SiC (f) samples.

Figure 7. Removal of different concentrations of Congo red dye using SiC, N-SiC, and NS-SiC catalysts (0.01 g catalyst, 10 ml dye, dark chamber, room temperature).

Figure 8. Proposed mechanism for catalytic performance of SiC catalysts.

Figure 9. Schematic structure of the different atoms on SiC samples and surface charges of atoms.

Figure 10. Control experiments of catalytic removal of Congo red (50 ppm) in dark condition with the addition of different radical quenchers.

Figure 11: Removal of Congo red (50 ppm) at different pH using NS-SiC (0.01 g catalyst, 10 ml dye, dark chamber, room temperature).

Figure 12. Removal of Congo red dye (100 ppm) using SiC, N-SiC, and NS-SiC catalysts (0.01 g catalyst, 10 ml dye, dark chamber, room temperature).

Figure 13. Recovery of SiC, N-SiC, and NS-SiC catalysts after 5 runs without washing the catalysts (a), and FT-IR spectra of used SiC catalysts (b) (0.01 g catalyst, 10 ml of 50 ppm dye, dark chamber, room temperature).

Figure 14. Recovery of NS-SiC catalyst after 5 runs after washing the catalyst (a), FT-IR spectra (b), and diffuse reflectance spectra of used and washed SiC catalyst (c) (0.01 g catalyst, 10 ml of 50 ppm dye, dark chamber, room temperature).

Figure 15. Comparison of the catalytic properties of SiC samples with their related carbon samples (0.01 g catalyst, 10 ml of 100 ppm dye, dark chamber, room temperature).

Figure 16. Comparison of the catalytic properties of NS-SiC sample in removal of different anionic azo dyes (0.01 g catalyst, 10 ml of 50 ppm dye, dark chamber, room temperature).

Table 1. Elemental analysis (atom%) of SiC samples.

Table 2. Textural characterization for the samples.

Table 3. Results of dye removal using SiC, N-SiC, and NS-SiC catalysts.

References

[1] Z. Cai, Y. Sun, W. Liu, F. Pan, P. Sun, J. Fu, An overview of nanomaterials applied for removing dyes from wastewater, Environ. Sci. Pollut. Res. 24 (2017) 15882-15904. doi.org/10.1007/s11356-017-9003-8.

[2] G.Z. Kyzas, K.A. Matis, Nanoadsorbents for pollutants removal: A review, J. Mol. Liq. 203 (2015) 159–168. doi.org/10.1016/j.molliq.2015.01.004.

[3] P.V. Nidheesh, M. Zhou, M. Oturan, A. An overview on the removal of synthetic dyes from water by electrochemical advanced oxidation processes, Chemosphere 197 (2018) 210-227. doi.org/10.1016/j.chemosphere.2017.12.195.

[4] X. Huan, R. Wang, T. Jiao, G. Zou, F. Zhan, J. Yin, L. Zhang, J. Zhou, Q. Peng, Facile Preparation of Hierarchical AgNP-Loaded MXene/Fe_3O4/ Polymer Nanocomposites by Electrospinning with Enhanced Catalytic Performance for Wastewater Treatment, ACS Omega 4 (2019) 1897−1906. doi.org/10.1021/acsomega.8b03615.

[5] S.V. Mohan, P. Ramaniah, N. Sharma, Biosorption of direct azo dye from aqueous phase onto Spirogyra sp. I02: Evaluation of kinetics and mechanistic aspects, Biochemical. Eng. J. 38 (2008) 61-69. doi.org/10.1016/j.bej.2007.06.014.

[6] A. Reife, H.S. Freeman, Environmental Chemistry of Dyes and Pigments, Wiley, U.S., 1996.

[7] F. Chen, E. Zhao, T. Kim, J. Wang, Gh. Hableel, P. James, T. Reardon, S.J. Ananthakrishna, T. Wang, S. Arconada-Alvarez, J.C. Knowles, J.V. Jokerst, Organosilica Nanoparticles with an Intrinsic Secondary Amine: An Efficient and Reusable Adsorbent for Dyes, ACS Appl. Mater. Interfaces, 9 (2017) 15566-15576. doi.org/10.1021/ acsami.7b04181.

[8] H. Wang, X. Yuan, Y. Wu, G. Zeng, X. Chen, L. Leng, H. Li, Synthesis and applications of novel graphitic carbon nitride/metal-organic frameworks mesoporous photocatalyst for dyes removal, Appl. Catal. B Environ. 174–175 (2015) 445–454. doi.org/10.1016/ j.apcatb.2015.03.037.

[9] J.L. Gong, B. Wang, G.M. Zeng, C.P. Yang, C.G. Niu, Q.Y. Niu, W.J. Zhou, Y. Liang, Removal of cationic dyes from aqueous solution using magnetic multi-wall carbon nanotube nanocomposite as adsorbent, J. Hazard. Mater. 164 (2009) 1517–1522. doi.org/10.1016/ j.jhazmat.2008.09.072.

[10] C. Varlikli, V. Bekiari, M. Kus, N. Boduroglu, I. Oner, P. Lianos, G. Lyberatos, S. Icli, Adsorption of dyes on Sahara desert sand. J. Hazard. Mater. 170 (2009) 27-34. doi.org/ 10.1016/j.jhazmat.2009.05.030.

[11] J. Zhu, R. Wang, R. Geng, X. Zhang, F. Wang, T. Jiao, J. Yang, Zh. Baic, Q. Peng, A facile preparation method for new two component supramolecular hydrogels and their performances in adsorption, catalysis, and stimuliresponse, RSC Adv. 9 (2019) 22551-22558. doi.org/ 10.1039/C9RA03827B.

[12] N. Hou, R. Wang, R.Geng, F. Wang, T. Jiao, L. Zhang, J. Zhou, Zh. Bai, Q. Peng, Facile preparation of self-assembled hydrogels constructed from poly-cyclodextrin and poly-adamantane as highly selective adsorbents for wastewater treatment, Soft Mat. 15 (2019) 6097-6106. doi.org/ 10.1039/C9SM00978G**.**

[13] X. Qin, F. Wang, S. Ren, L. Yang, Y. Meng, L. Sun, Self-forming salt-assisted synthesis of SiC nanoparticles and their adsorption property for methylene blue from aqueous solution, Ceram. Int. (2015) 1001–1015. doi.org/10.1016/ j.ceramint.2015.09.008.

[14] E. Ghasemian Lemraski, Z. Tahmasebi, Zero valent iron loaded on SiC nanoparticles as a new adsorbent for removing Pb (lead) and azo dyes from aqueous solution, Environ. Prog. Sustain. Energy 37 (2018) 1657-1667. doi.org/10.1002/ep.12849.

[15] Y. Mao, Sh. Yang, Ch. Xue, M. Zhang, W. Wang, Zh. Song, X. Zhao, J. Sun, Rapid degradation of malachite green by $CoFe_2O_4$–SiC foam under microwave radiation, R. Soc. Open Sci. 5 (2018) 180085. doi.org/10.1098/rsos.180085.

[16] L.V. Bora, R.K. Mewada, Photocatalytic treatment of dye wastewater and parametric study using a novel Z-scheme Ag_2CO_3/SiC photocatalyst under natural sunlight, J. Environ. Chem. Eng.5 (2017) 5556-5565. doi.org/10.1016/j.jece.2017.10.037.

[17] A. Dubey, P. Khosla, H.K. Singh, V. Katoch, D. Kumar, P. Gupta, A review on role of processing parameter in determining properties of silicon carbide reinforced Metal Matrix Nanocomposites, J. Appl. Sci. Eng. 19 (2016) 303–312. doi.org/10.6180/jase.2016.19.3.08.

[18] J. Fan, P.K. Chu, Silicon Carbide Nanostructures, Springer, Cham, 2014.

[19] R. Wu, K. Zhou, C.Y. Yue, J. Wei, Y. Pan, Recent progress in synthesis, properties and potential applications of SiC nanomaterials, Prog. Mater. Sci. 72 (2015) 1–60. Doi.org/10.1016/j.pmatsci.2015.01.003.

[20] M. Afsharpour, E. Khomand, Synthesis of Bio-inspired Porous Silicon Carbides using Cortaderia Selloana and Equisetum Arvense Grasses as Remarkable Sulfur Adsorbents, Int. J. Environ. Sci. Technol. 16 (2019) In Press. doi.org/10.1007/s13762-018-1679-x.

[21] H. Pan, H. Hou, Y. Shi, H. Li, J. Chen, L. Wang, J.C. Crittenden, High catalytic oxidation of As(III) by molecular oxygen over Fe-loaded silicon carbide with MW

activation, Chemosphere 198 (2018) 537-545. doi.org/10.1016/ j.chemosphere.2018.01.116.

[22] E. Khomand, M. Afsharpour, Green Synthesis of SiCs by using Natural Gums (Guar, Tragacanth, Arabic and Xanthan) for Desulfurization of Model Fuel, Int. J. Environ. Sci. Technol. 16 (2019) In Press. doi.org/10.1007/s13762-018-1678-y.

[23] S.E. Saddow, Silicon Carbide Biotechnology: A Biocompatible Semiconductor for Advanced Biomedical Devices and Applications: Elsevier Inc, (2016) 1-356. doi.org/10.1016/C2014-0-03629-5.

[24] M. Afsharpour, A.R. Amraee, Synthesis of bio-inspired N-doped SiC and investigation of its synergetic effects on Mo catalysts in oxidative desulfurization reaction, Mol. Catal. 436 (2017) 285–293. doi.org/10.1016/j.mcat.2017.04.029.

[25] H. Dong, B. Lin, K. Gilmore, T. Hou, S.T. Lee, Y. Li, Theoretical investigations on SiC siligraphene as promising metal-free catalyst for oxygen reduction reaction, J. Power Sources. 299 (2015) 371–379. doi.org/10.1016/j.jpowsour.2015.09.014.

[26] X.Y. Guo, G.Q. Jin, Pore-size control in the sol-gel synthesis of mesoporous silicon carbide, J. Mater. Sci. 40 (2005) 1301–1303. doi:10.1007/s10853-005-6957-6.

[27] J. Park, Y. Kim, M. Jung, Preparation of Porous SiC Ceramics Using Polycarbosilane Derivatives as Binding Agents, J. Korea. Ceram. Soc. 49 (2012) 412-416. doi.org/10.4191/kcers.2012.49.5.412.

[28] M. Dasog, L.F. Smith, T.K. Purkait, J.G.C. Veinot, Low temperature synthesis of silicon carbide nanomaterials using a solid-state method, Chem. Commun. 49 (2013) 7004. doi.org/10.1039/c3cc43625j.

[29] B. Zhao, H. Zhang, H. Tao, Z. Tan, Z. Jiao, M. Wu, Low temperature synthesis of

mesoporous silicon carbide via magnesiothermic reduction, Mater. Lett. 65 (2011) 1552–1555. doi.org/10.1016/j.matlet.2011.02.075.

[30] C. Liu, D. Yu, D.W. Kirk, Y. Xu, Porous silicon carbide derived from apple fruit with high electromagnetic absorption performance, J. Mater. Chem. C. 4 (2016) 5349–5356. doi.org/10.1039/C6TC01319H.

[31] I. Anastopoulos, A. Hosseini-Bandegharaei, J. Fu, A.C. Mitropoulos, G.Z. Kyzas, Use of nanoparticles for dye adsorption: Review, J. Dispers. Sci. Technol. 39 (2018) 836-848. doi.org/10.1080/01932691.2017.1398661.

[32] H. Dong, L. Zhou, T. Frauenheim, T. Hou, S.-T. Lee, Y. Li, SiC $_7$ siligraphene: a novel donor material with extraordinary sunlight absorption, Nanoscale. 8 (2016) 6994–6999. doi.org/10.1039/C6NR00046K.

[33] H. Dong, L. Wang, L. Zhou, T. Hou, Y. Li, Theoretical investigations on novel SiC5siligraphene as gas sensor for air pollutants, Carbon N. Y. 113 (2017) 114–121. doi.org/10.1016/j.carbon.2016.11.029.

[34] L.J. Zhou, Y.F. Zhang, L.M. Wu, SiC_2 siligraphene and nanotubes: Novel donor materials in excitonic solar cells, Nano Lett. 13 (2013) 5431–5436. doi.org/10.1021/nl403010s.

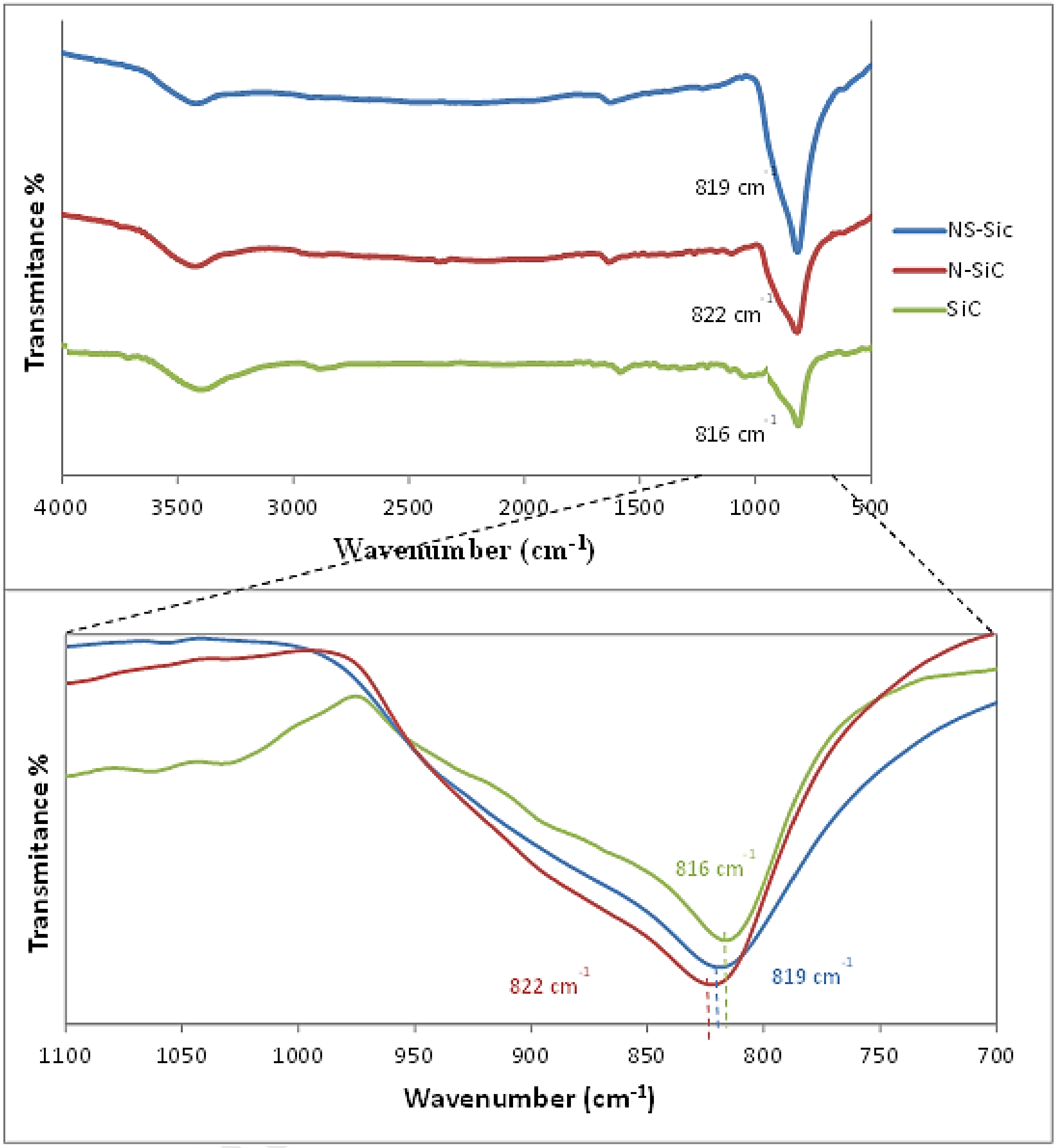
Transmitance %
819 cm-1
822 cm-1
816 cm-1
NS-Sic
N-SiC
SiC
4000
3500
3000
2500
2000
1500
1000
500
Wavenumber (cm-1)
Transmitance %
816 cm-1
822 cm-1
819 cm-1
1100
1050
1000
950
900
850
800
750
700
Wavenumber (cm-1)

Fig. 1

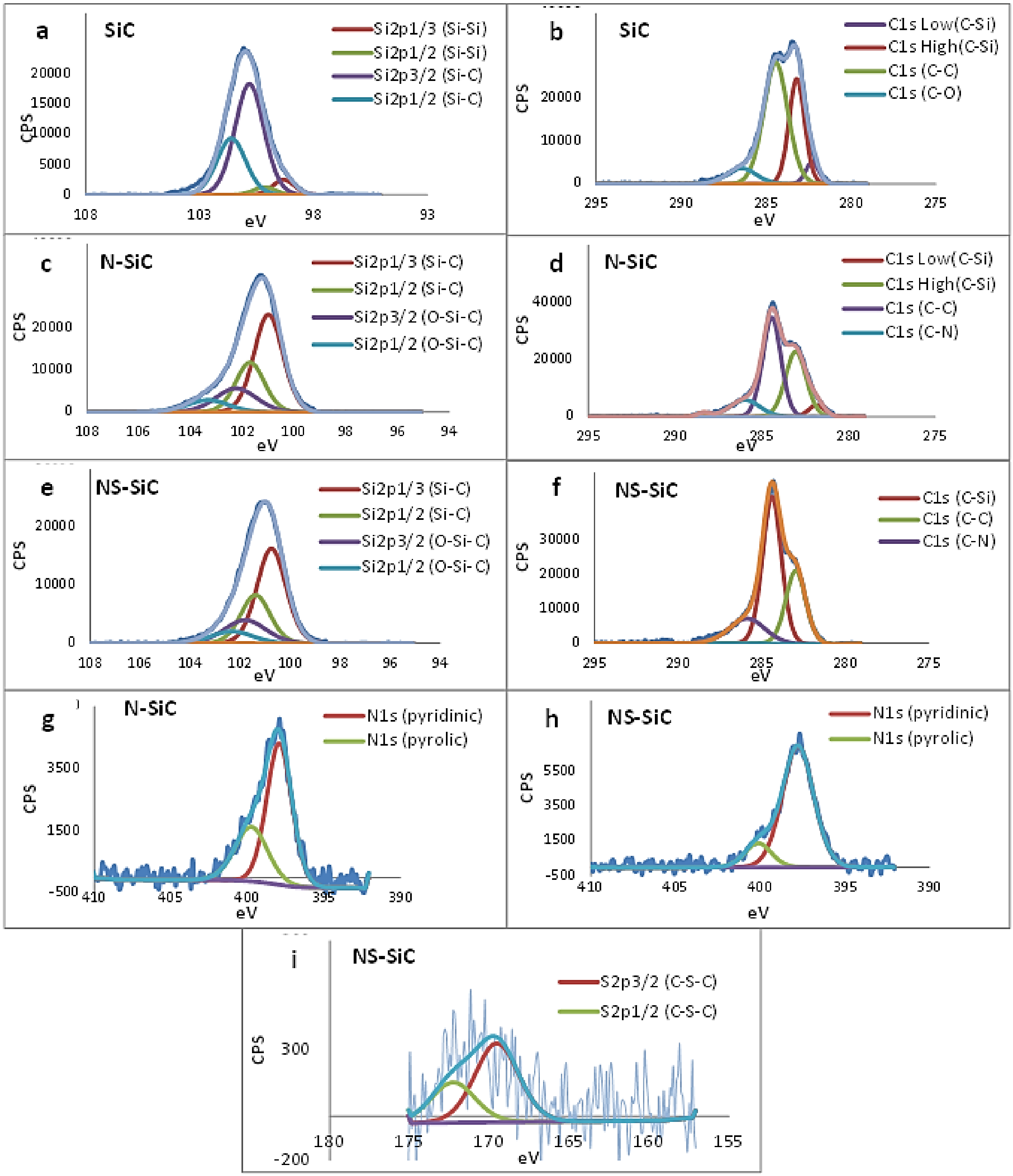
a
SiC
Si2p1/3 (Si-Si)
Si2p1/2 (Si-Si)
Si2p3/2 (Si-C)
Si2p1/2 (Si-C)
CPS
20000
15000
10000
5000
0
108
103
98
93
eV
b
SiC
C1s Low(C-Si)
C1s High(C-Si)
C1s (C-C)
C1s (C-O)
CPS
20000
10000
0
295
290
285
280
275
eV
c
N-SiC
Si2p1/3 (Si-C)
Si2p1/2 (Si-C)
Si2p3/2 (O-Si-C)
Si2p1/2 (O-Si-C)
CPS
20000
10000
0
108
106
104
102
100
98
96
94
eV
d
N-SiC
C1s Low(C-Si)
C1s High(C-Si)
C1s (C-C)
C1s (C-N)
CPS
40000
20000
0
295
290
285
280
275
eV
e
NS-SiC
Si2p1/3 (Si-C)
Si2p1/2 (Si-C)
Si2p3/2 (O-Si-C)
Si2p1/2 (O-Si-C)
CPS
20000
10000
0
108
106
104
102
100
98
96
94
eV
f
NS-SiC
C1s (C-Si)
C1s (C-C)
C1s (C-N)
CPS
30000
20000
10000
0
295
290
285
280
275
eV
g
N-SiC
N1s (pyridinic)
N1s (pyrolic)
CPS
3500
1500
-500
410
405
400
395
390
eV
h
NS-SiC
N1s (pyridinic)
N1s (pyrolic)
CPS
5500
3500
1500
-500
410
405
400
395
390
eV
i
NS-SiC
S2p3/2 (C-S-C)
S2p1/2 (C-S-C)
CPS
300
-200
180
175
170
165
160
155
eV

Fig. 2

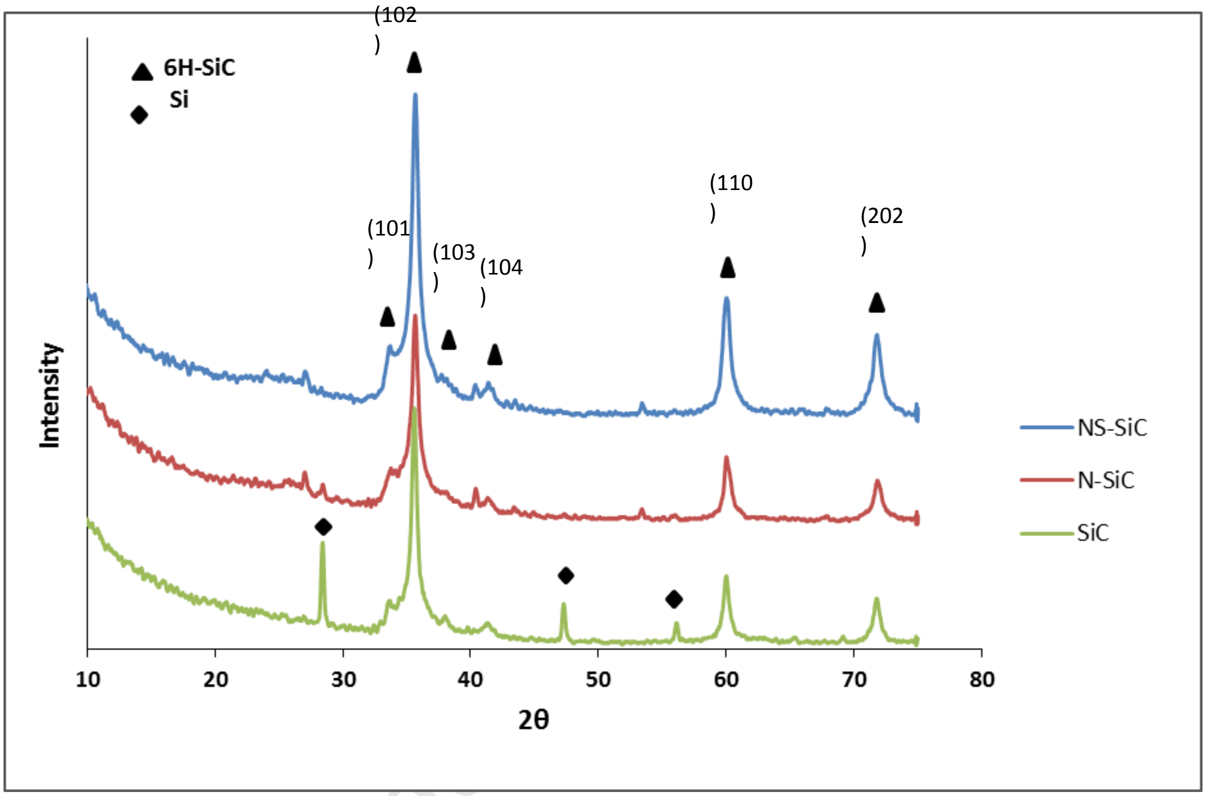
▲ 6H-SiC
◆ Si
(102)
(101)
(103)
(104)
(110)
(202)
Intensity
2θ
10
20
30
40
50
60
70
80
NS-SiC
N-SiC
SiC

Fig. 3

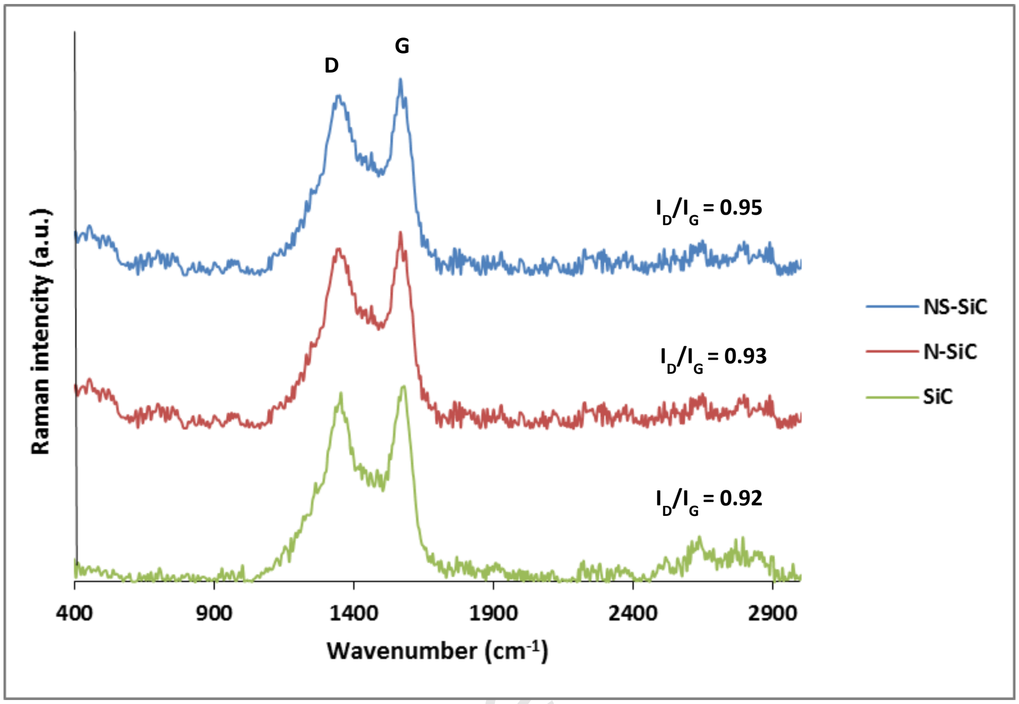
D
G
$I_D/I_G = 0.95$
$I_D/I_G = 0.93$
$I_D/I_G = 0.92$
NS-SiC
N-SiC
SiC
Raman intencity (a.u.)
400
900
1400
1900
2400
2900
Wavenumber (cm^{-1})

Fig. 4

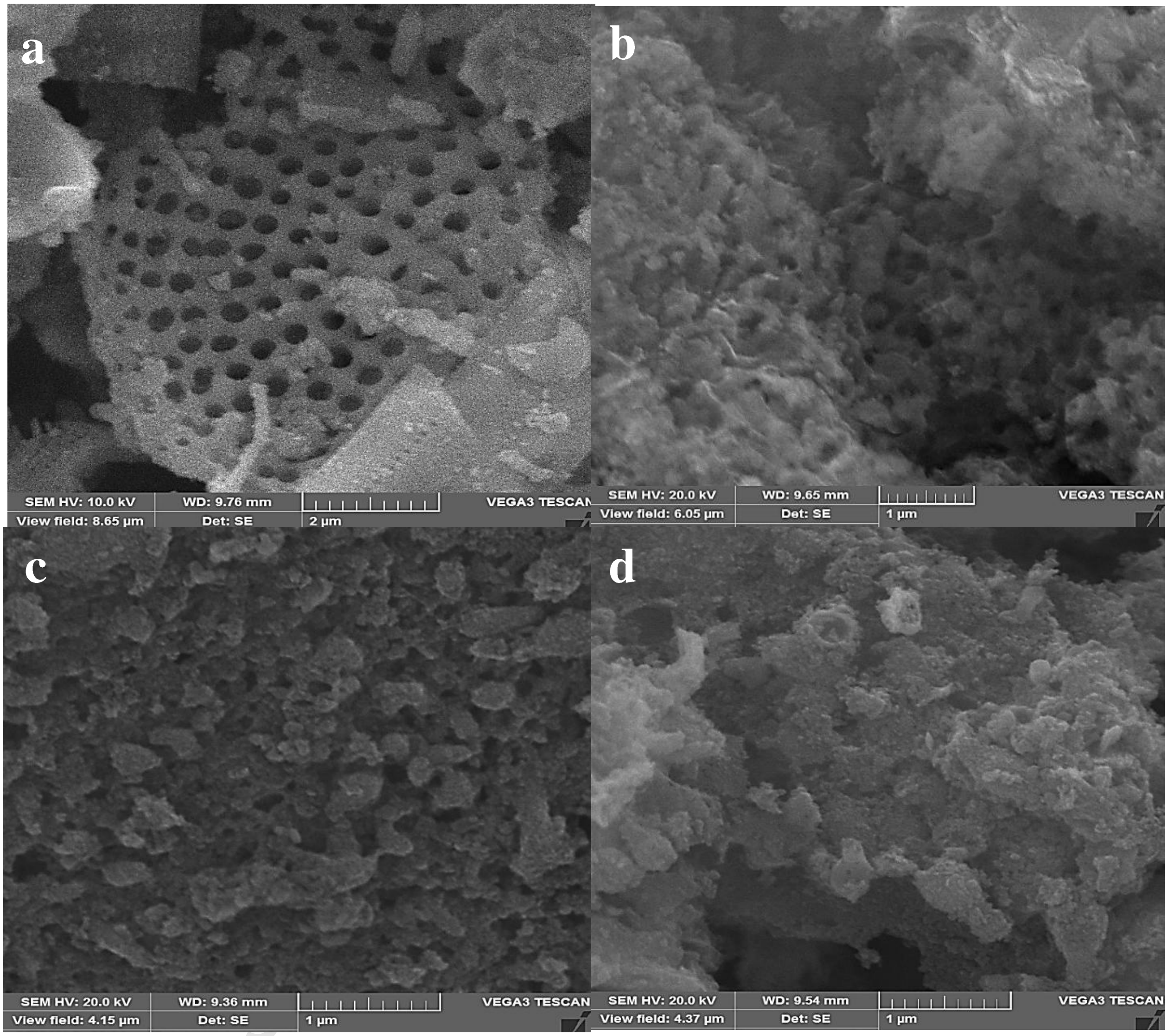
a
SEM HV: 10.0 kV
WD: 9.76 mm
VEGA3 TESCAN
View field: 8.65 µm
Det: SE
2 µm
b
SEM HV: 20.0 kV
WD: 9.65 mm
VEGA3 TESCAN
View field: 6.05 µm
Det: SE
1 µm
c
SEM HV: 20.0 kV
WD: 9.36 mm
VEGA3 TESCAN
View field: 4.15 µm
Det: SE
1 µm
d
SEM HV: 20.0 kV
WD: 9.54 mm
VEGA3 TESCAN
View field: 4.37 µm
Det: SE
1 µm

Fig. 5

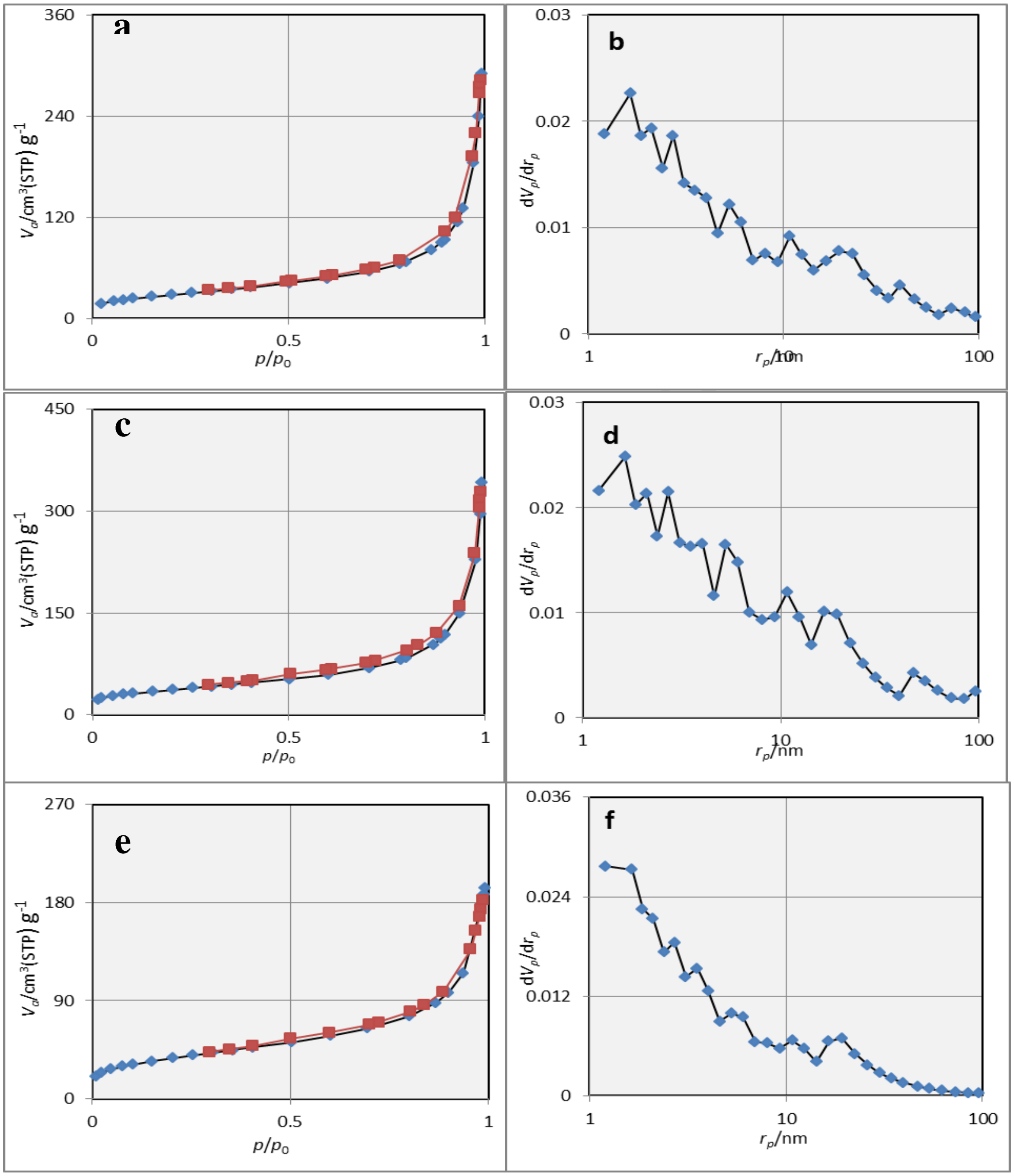
a
360
240
120
0
0
0.5
1
V_a/cm^3(STP) g^{-1}
p/p_0
b
0.03
0.02
0.01
0
1
10
100
dV_p/dr_p
r_p/nm
c
450
300
150
0
0
0.5
1
V_a/cm^3(STP) g^{-1}
p/p_0
d
0.03
0.02
0.01
0
1
10
100
dV_p/dr_p
r_p/nm
e
270
180
90
0
0
0.5
1
V_a/cm^3(STP) g^{-1}
p/p_0
f
0.036
0.024
0.012
0
1
10
100
dV_p/dr_p
r_p/nm

Fig. 6

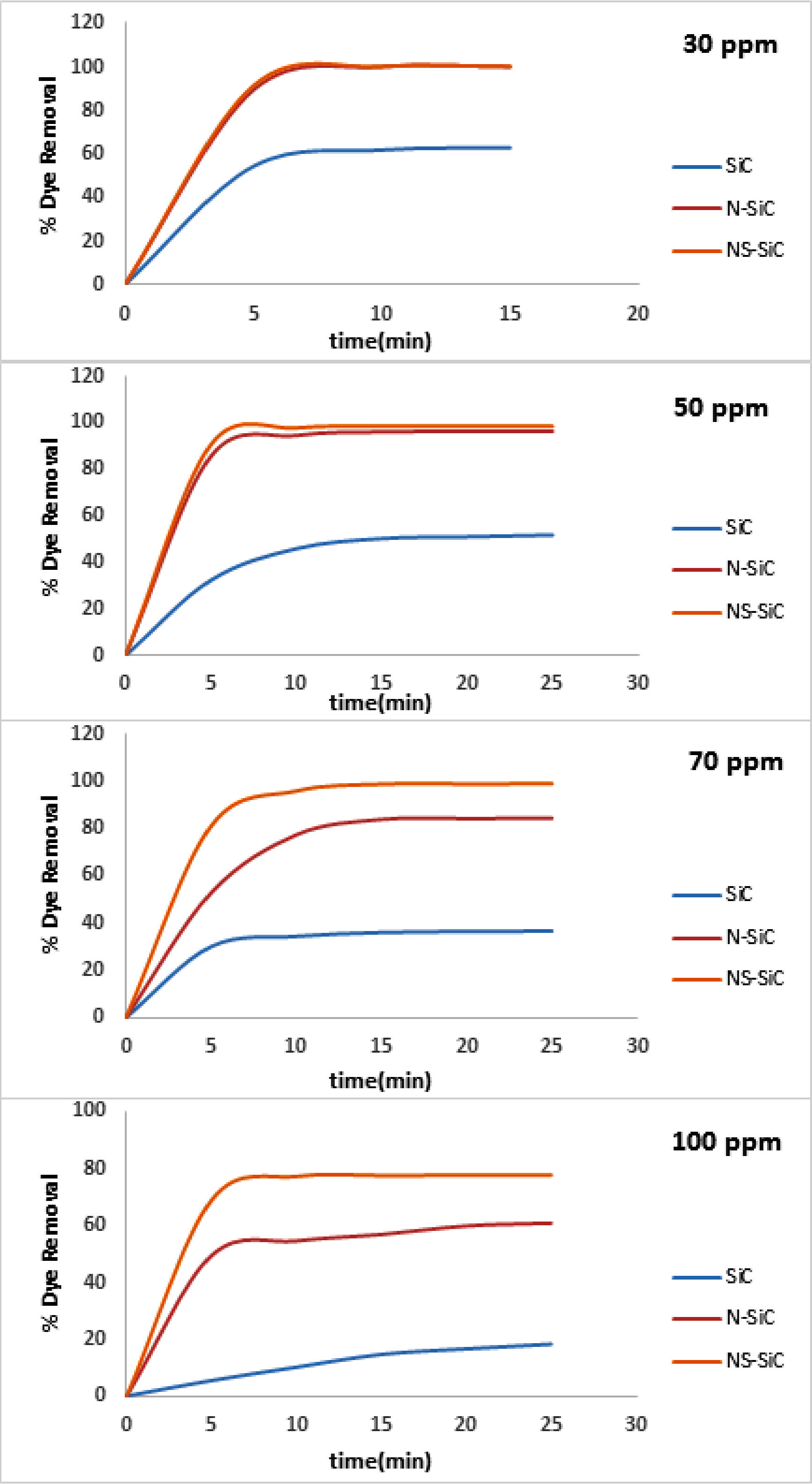
30 ppm
% Dye Removal
120
100
80
60
40
20
0
0
5
10
15
20
time(min)
SiC
N-SiC
NS-SiC
50 ppm
% Dye Removal
120
100
80
60
40
20
0
0
5
10
15
20
25
30
time(min)
SiC
N-SiC
NS-SiC
70 ppm
% Dye Removal
120
100
80
60
40
20
0
0
5
10
15
20
25
30
time(min)
SiC
N-SiC
NS-SiC
100 ppm
% Dye Removal
100
80
60
40
20
0
0
5
10
15
20
25
30
time(min)
SiC
N-SiC
NS-SiC

Fig. 7

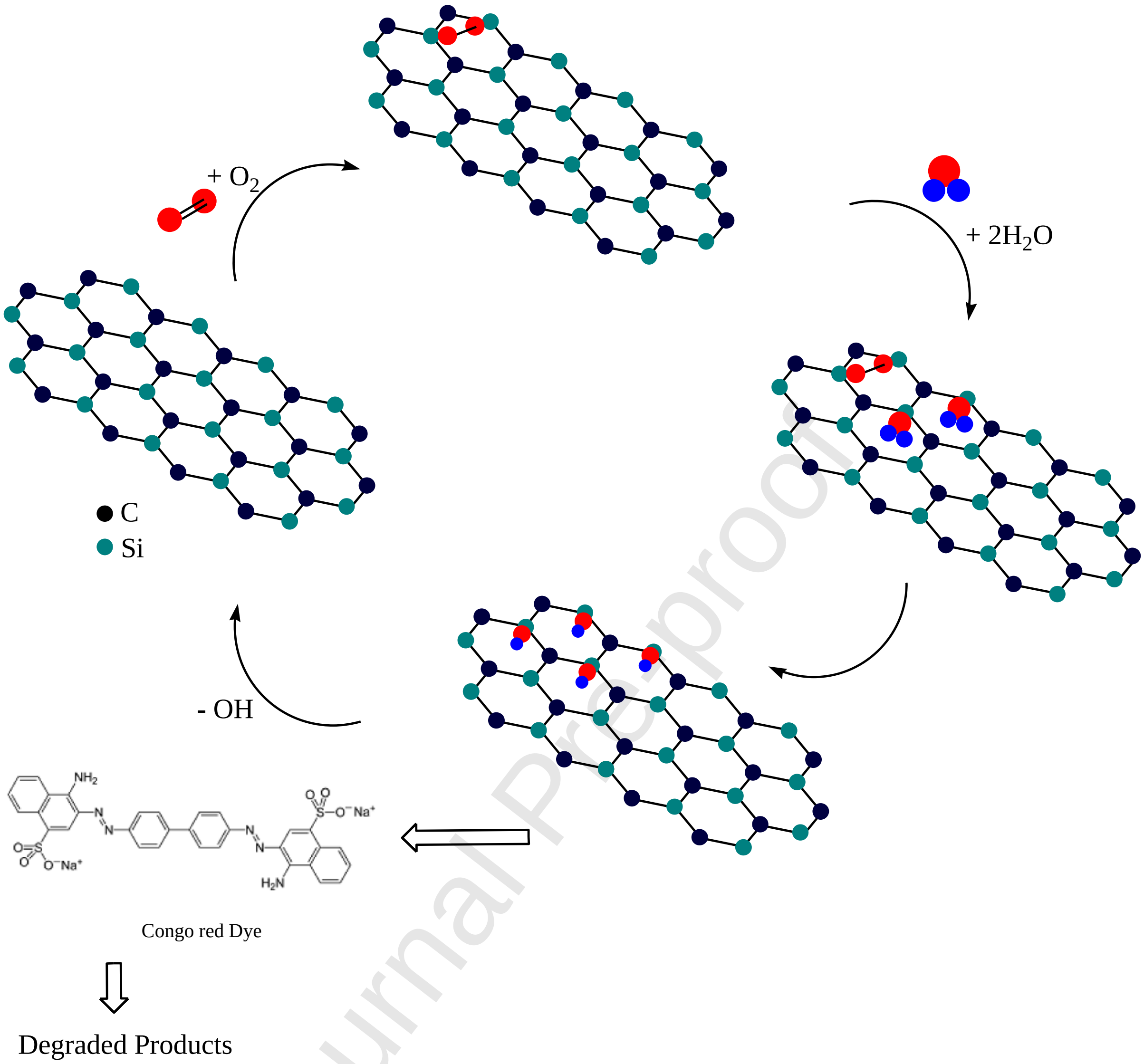

+ O$_2$
+ 2H$_2$O
● C
● Si
- OH
NH$_2$
H$_2$N
N
O
S
O$^-$ Na$^+$
Congo red Dye
Degraded Products

Fig. 8

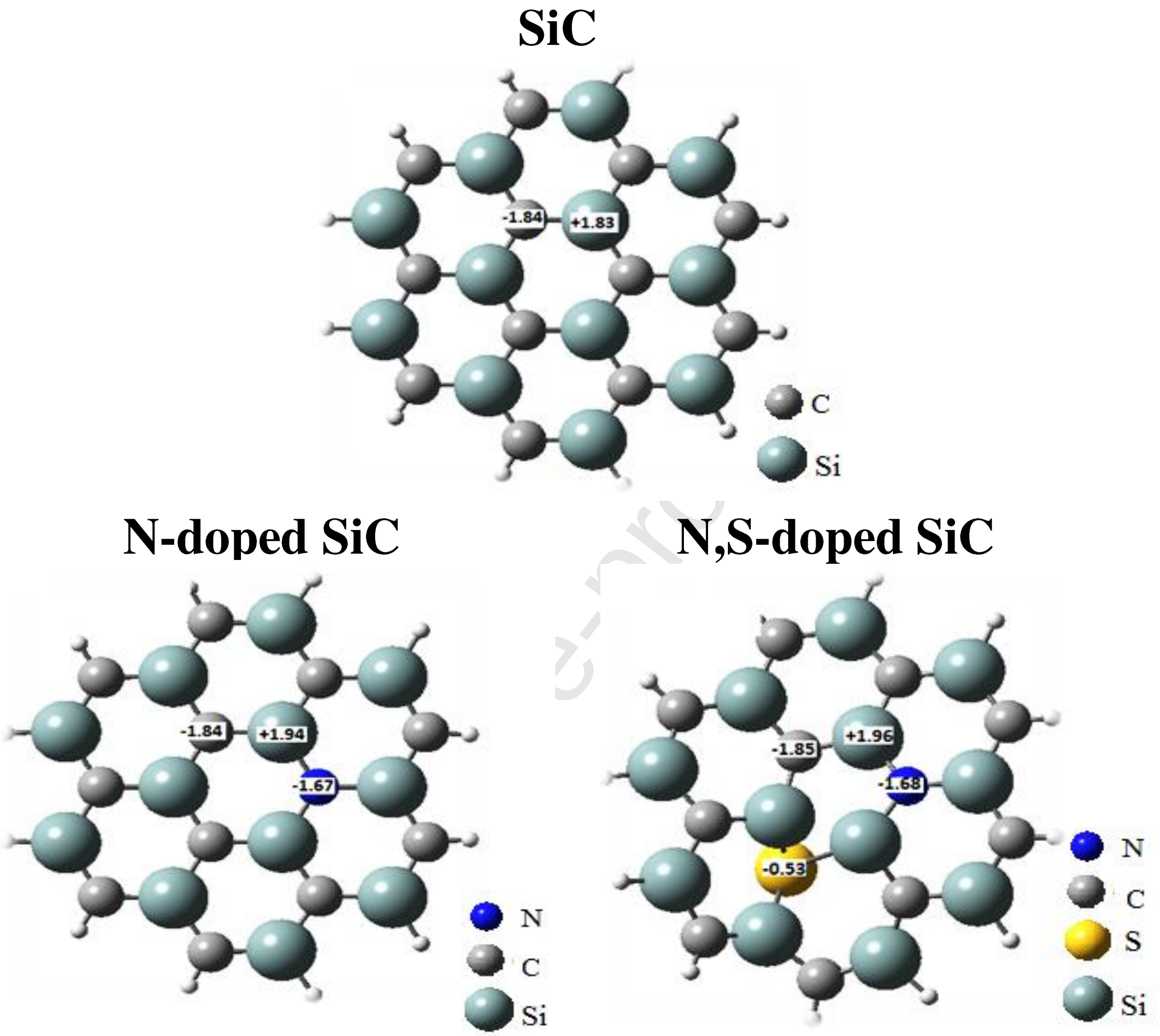
SiC

N-doped SiC

N,S-doped SiC

Fig. 9

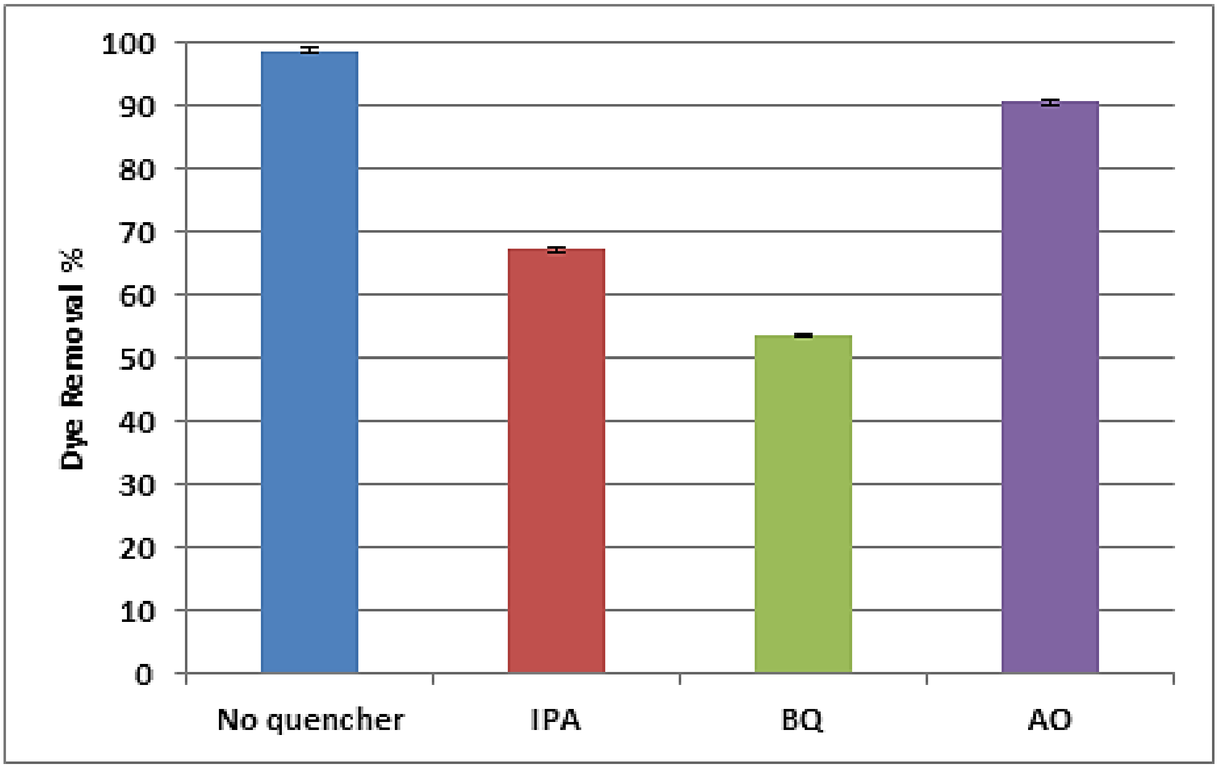

Fig. 10

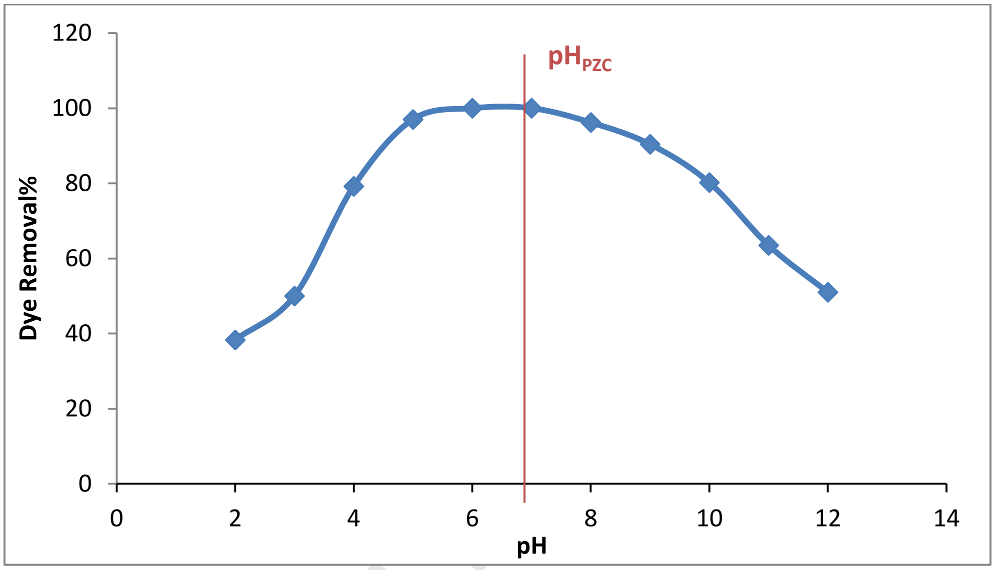

Fig. 11

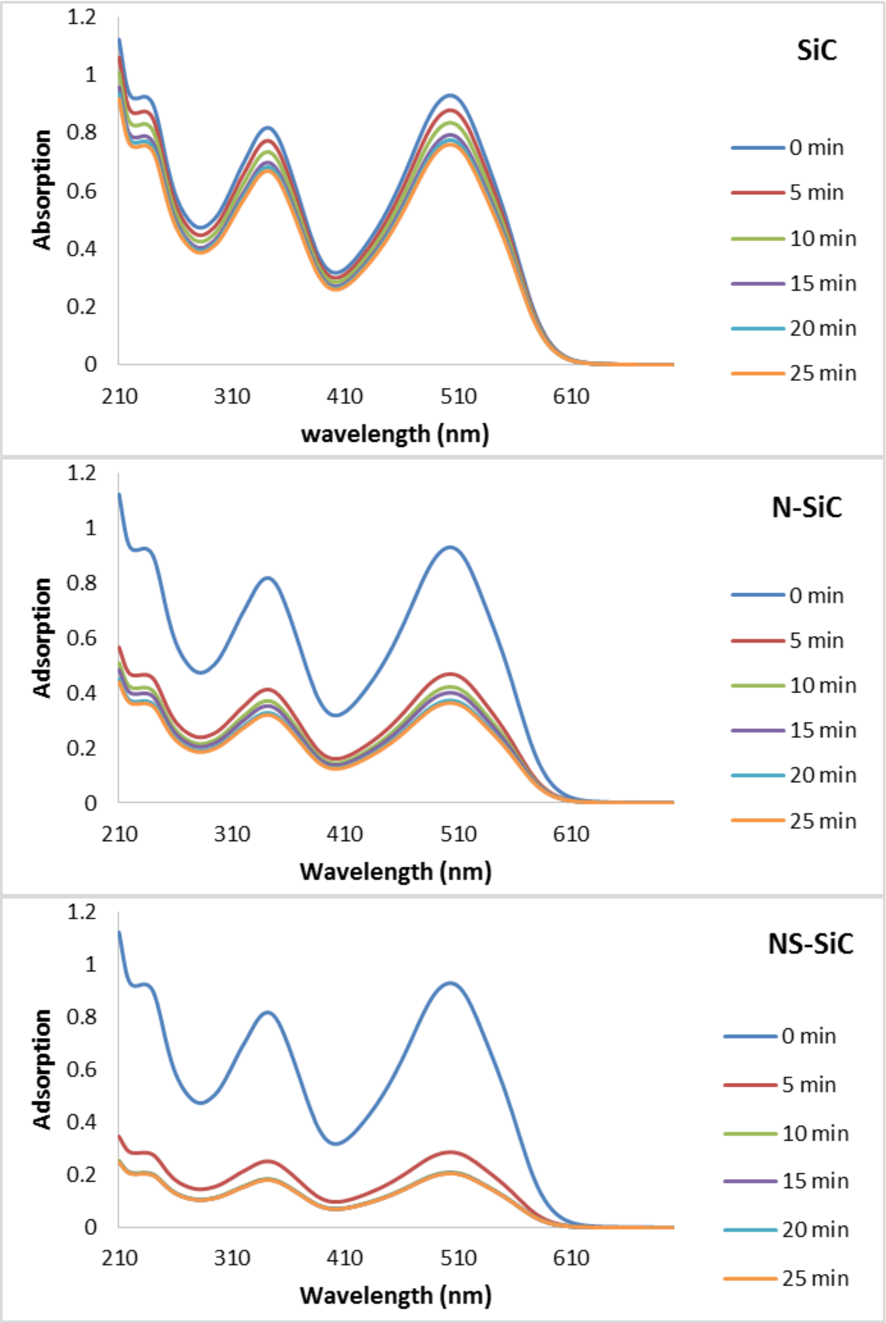
SiC
Absorption
1.2
1
0.8
0.6
0.4
0.2
0
210
310
410
510
610
wavelength (nm)
0 min
5 min
10 min
15 min
20 min
25 min
N-SiC
Adsorption
1.2
1
0.8
0.6
0.4
0.2
0
210
310
410
510
610
Wavelength (nm)
0 min
5 min
10 min
15 min
20 min
25 min
NS-SiC
Adsorption
1.2
1
0.8
0.6
0.4
0.2
0
210
310
410
510
610
Wavelength (nm)
0 min
5 min
10 min
15 min
20 min
25 min

Fig. 12

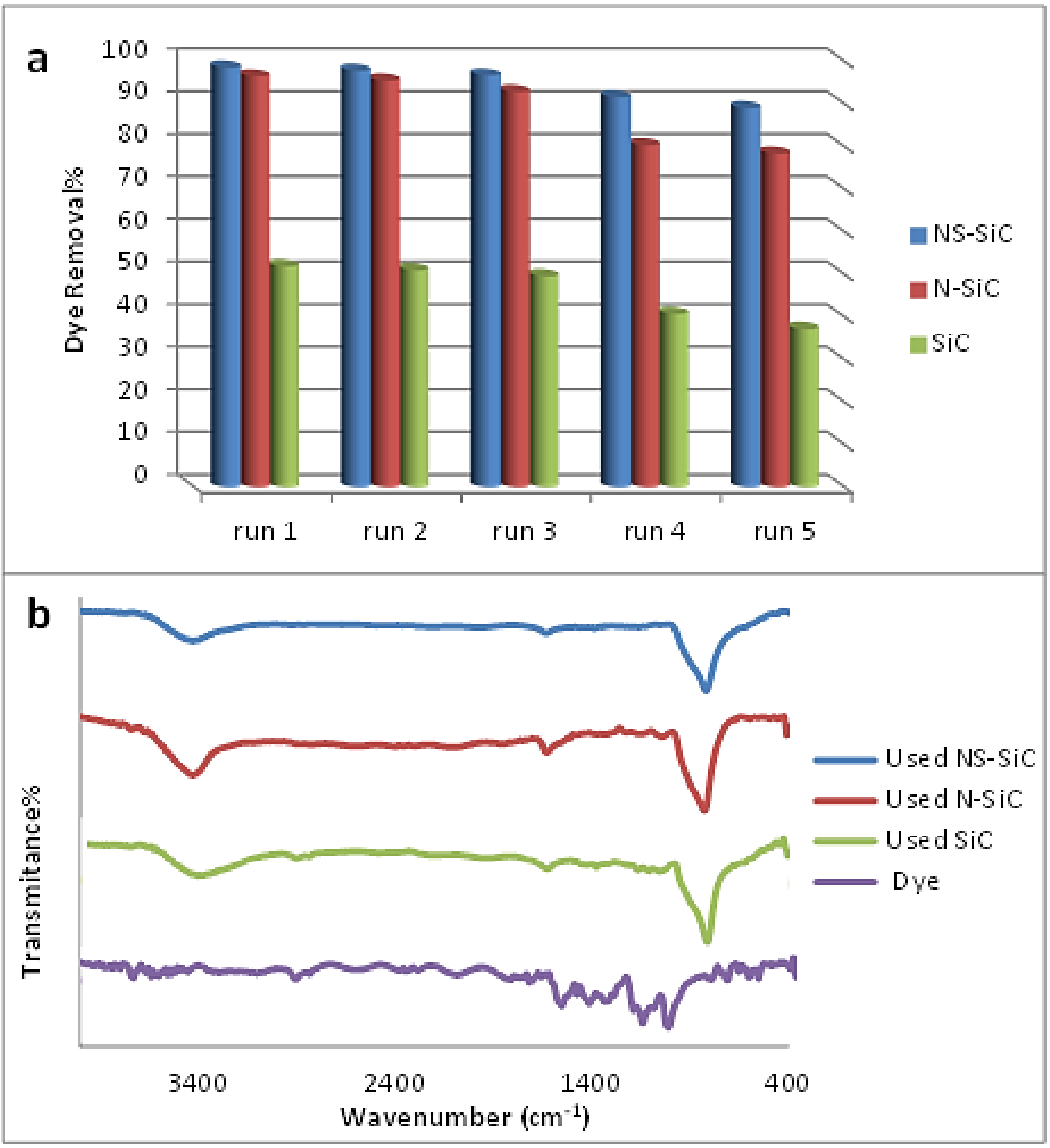
a
Dye Removal%
100
90
80
70
60
50
40
30
20
10
0
run 1
run 2
run 3
run 4
run 5
NS-SiC
N-SiC
SiC
b
Transmitance%
3400
2400
1400
400
Wavenumber (cm-1)
Used NS-SiC
Used N-SiC
Used SiC
Dye

Fig. 13

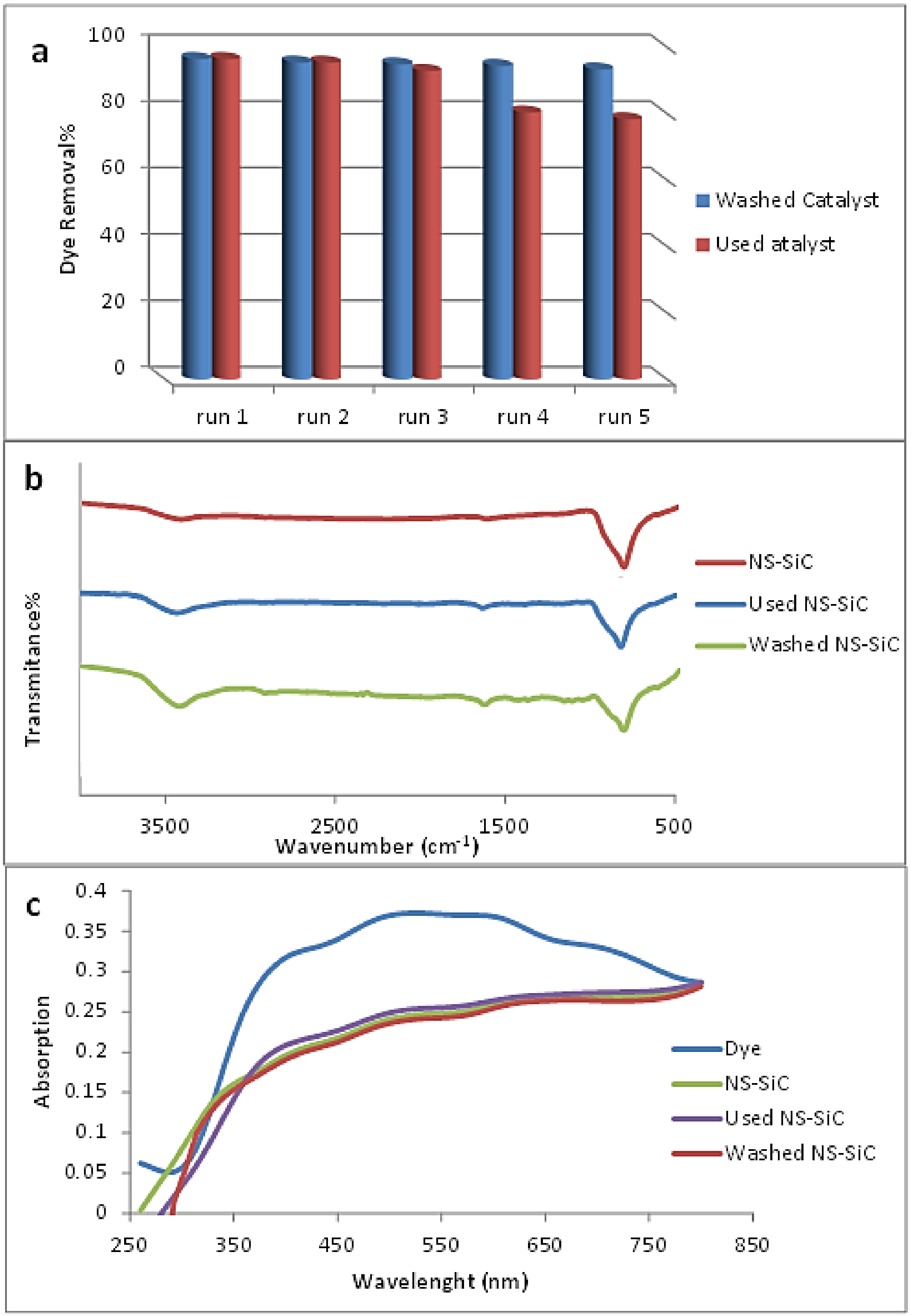
a
100
80
60
40
20
0
Dye Removal%
run 1
run 2
run 3
run 4
run 5
Washed Catalyst
Used atalyst
b
Transmitance%
NS-SiC
Used NS-SiC
Washed NS-SiC
3500
2500
1500
500
Wavenumber (cm-1)
c
0.4
0.35
0.3
0.25
0.2
0.15
0.1
0.05
0
Absorption
250
350
450
550
650
750
850
Wavelenght (nm)
Dye
NS-SiC
Used NS-SiC
Washed NS-SiC

Fig. 14

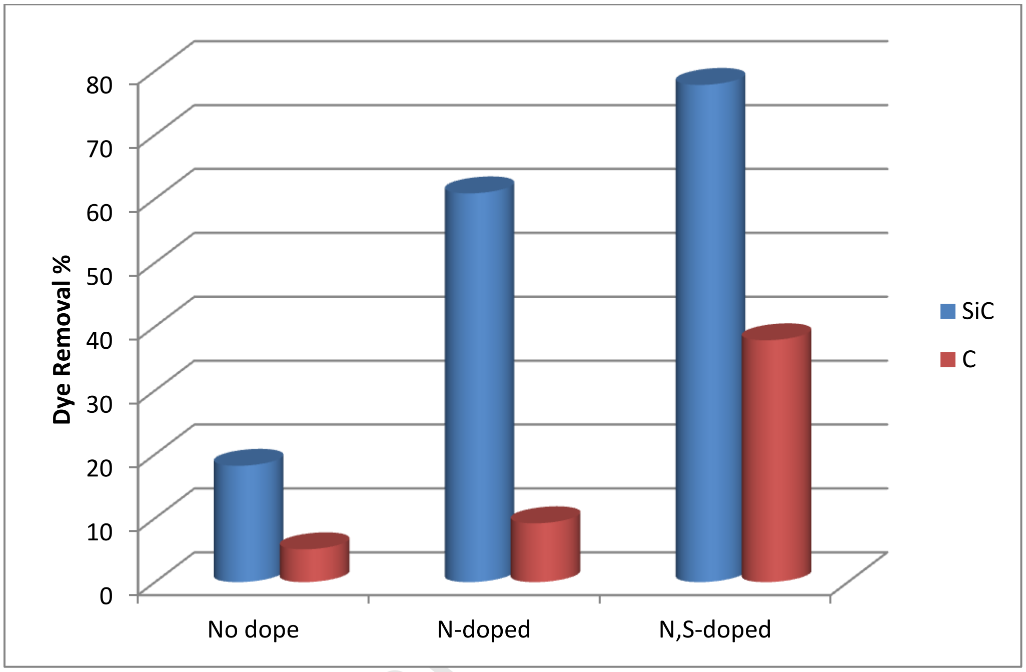
Dye Removal %
0
10
20
30
40
50
60
70
80
No dope
N-doped
N,S-doped
SiC
C

Fig. 15

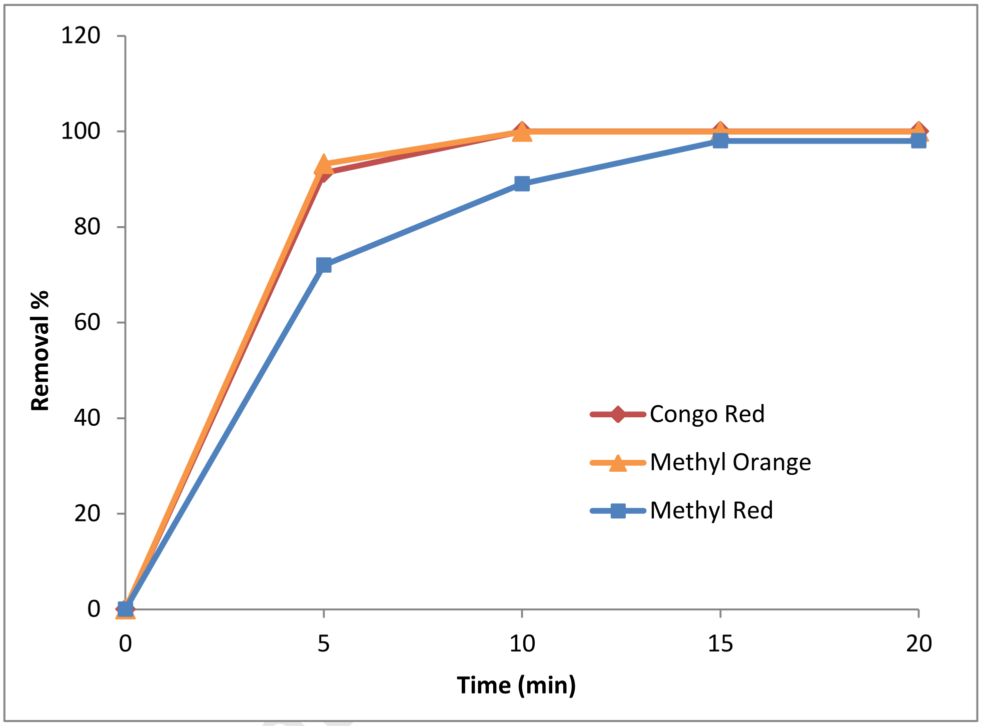
120
100
80
60
40
20
0
Removal %
0
5
10
15
20
Time (min)
Congo Red
Methyl Orange
Methyl Red

Fig. 16

Table 1

Element	**EDX (atom%)**			**XPS (atom%)**		
	SiC	**N-SiC**	**NS-SiC**	**SiC**	**N-SiC**	**NS-SiC**
Si	30.46	30.47	19.38	32.37	36.31	27.84
C	57.16	45.27	57.96	58.83	45.44	57.69
O	9.89	15.24	7.31	8.79	14.21	8.27
N	_	6.21	8.02	-	4.05	5.66
S	_	_	0.32	-		0.54

Table 2

Sample	S_{BET} (m^2/g)[a]	Total Pore Volume (cm^3/g)[b]	Micropore Volume (cm^3/g)[c]	Mesopore Volume (cm^3/g)	Average Pore Diameter (nm)[a]	Content %[c]	
						Micropore	Mesopore
SiC	101	0.428	0.001	0.427	16.98	0.24	99.76
N-SiC	135	0.487	0.001	0.486	14.49	0.26	99.74
NS-SiC	133	0.291	0.043	0.248	8.76	14.73	85.27

[a] were determined by using the BET theory, [b] was measured by BJH method, and [c] were evaluated by the t-plot method.

Table 3

Sample	Dye Concentration (ppm)	Catalyst Amount (g)	Time (min)	C_e	Q_e	Removal (%)
SiC	30	0.01	15	11.17	18.83	62.76
N-SiC	30	0.01	10	0.01	29.98	99.95
NS-SiC	30	0.01	10	1.41	29.99	99.99
SiC	50	0.01	25	24.05	47.83	51.88
N-SiC	50	0.01	20	1.75	70.13	96.48
NS-SiC	50	0.01	20	0.69	71.19	98.60
SiC	70	0.01	25	44.44	39.95	36.50
N-SiC	70	0.01	20	11.06	73.34	84.19
NS-SiC	70	0.01	20	0.85	83.55	98.78
SiC	100	0.01	25	81.78	28.29	18.21
N-SiC	100	0.01	25	39.14	70.93	60.85
NS-SiC	100	0.01	25	22.16	87.91	77.83
NS-SiC	30	0.1	5	0	30.00	100
NS-SiC	30	0.05	20	0.09	59.82	99.70
NS-SiC	30	0.005	30	5.39	49.22	82.03

Graphical abstract

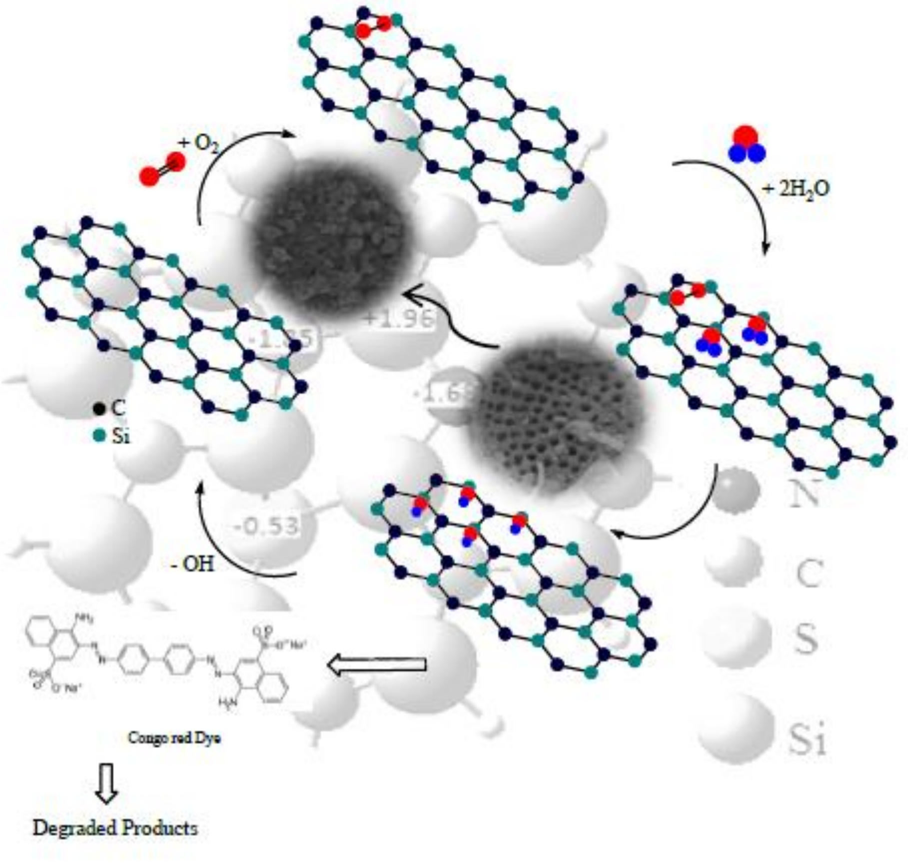

Highlights

- Doped siligraphenes are the high-performance catalysts in oxidation reactions.
- Siligraphenes are the good catalysts for degradation of dyes under dark condition.
- Doping increases the surface area and defects to enhance the adsorption of dye.
- Positive charged Si atoms in doped SiC adsorbed oxygen for radical degradation.
- Doped siligraphenes display good stability even in continues reaction.